

Measurement of the nonlinear refractive index of air constituents at mid-infrared wavelengths

S. Zahedpour, J. K. Wahlstrand, and H. M. Milchberg

Institute for Research in Electronics and Applied Physics, University of Maryland, College Park, MD 20742

We measure the nonlinear refractive index coefficients in N_2 , O_2 and Ar from visible through mid-infrared wavelengths ($\lambda = 0.4 - 2.4 \mu\text{m}$). The wavelengths investigated correspond to transparency windows in the atmosphere. Good agreement is found with theoretical models of $\chi^{(3)}$. Our results are essential for accurately simulating the propagation of ultrashort mid-IR pulses in the atmosphere.

Filamentary propagation of intense ultrashort laser pulses in atmosphere for $\lambda < \sim 1 \mu\text{m}$ has been a subject of extensive study [1, 2], finding applications in the generation of terahertz radiation [3], high harmonic generation [4], air lasing [5-7], and remote inscription of optical waveguides into air [8–13]. It has been anticipated that new regimes of laser filamentation are possible at longer wavelengths, such as in the mid-infrared (mid-IR, $\lambda \sim 1.5\text{-}10 \mu\text{m}$), where beam collapse arrest may occur through harmonic walk-off rather than plasma-induced refraction [14]. Mid-IR filamentation is effective for generating coherent keV-level photon beams in high pressure gas-filled capillaries [15] and broad mid-IR supercontinua in high pressure gas volumes [16].

Accurate values for nonlinear coefficients are essential for high fidelity simulations of intense laser propagation [17]—such simulations are indispensable not only for designing experiments and informing applications, but they also motivate the design and parameters of the lasers themselves. We recently showed that in the near-infrared (pump wavelength $\lambda_e = 0.8 \mu\text{m}$), air propagation simulations depend very sensitively on the values used for the coefficients (n_2) describing the instantaneous electronic nonlinear response of air constituents [18]. Best agreement of the simulations with axially resolved measurements occurs for n_2 coefficients measured in [19].

In this Article, we present measurements of n_2 for the air constituents N_2 , O_2 and Ar at pump wavelengths ranging from 400 nm to 2400 nm. The near through mid-IR wavelengths chosen ($\lambda_e = 1250 \text{ nm}, 1650 \text{ nm}, 2200 \text{ nm}, 2400 \text{ nm}$) are within the transparency windows of air [20]. We find that the nonlinear response is quite dispersionless over the range of wavelengths investigated, except near $\lambda_e=400 \text{ nm}$, consistent with a simple model for the third-order nonlinear susceptibility developed by Bishop [21].

The experimental setup is shown in Fig 1. Pulses from a 1 kHz Ti:Sapphire regenerative amplifier centered at 800 nm are split, with 2.8 mJ pumping an optical parametric amplifier (OPA) [22], which is tunable from 1100 nm to 2600 nm. A chopper reduces the pulse repetition rate to 500 Hz. The remaining portion of the 800 nm pulse is attenuated and weakly focused in a 2 atm xenon gas cell, where filamentation generates a $\lambda=500\text{--}700 \text{ nm}$ broadband supercontinuum (SC) transmitted through the pump-rejecting dichroic splitter. A Michelson interferometer splits the SC into two collinear pulses (reference and probe) temporally separated by 2 ps. The dispersive glass in the SC beam path introduces equal positive chirp to $\sim 1.5 \text{ ps}$ on the reference and probe. The OPA output pulse and the SC reference/probe are focused in a backfilled chamber, crossing at 2° .

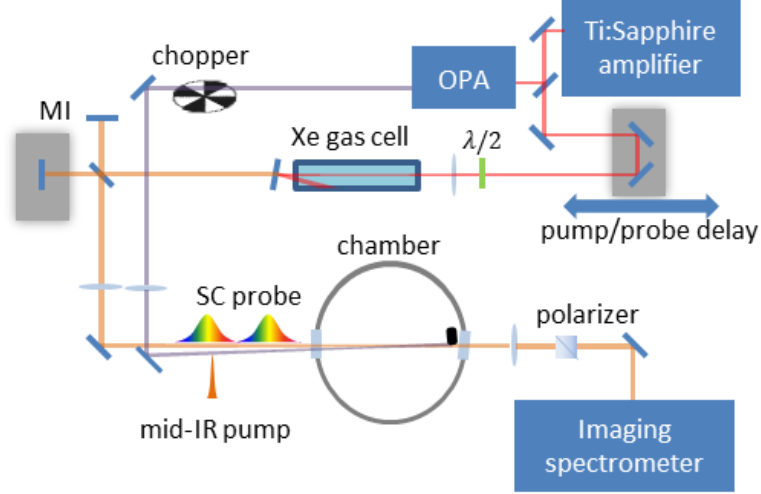


Fig. 1. Diagram of the experiment. A Ti:sapphire regenerative amplifier pumps an infrared optical parametric amplifier (OPA) to produce a tunable pump pulse and generates visible supercontinuum (SC) in a Xe gas cell. A Michelson interferometer (MI) creates probe and reference SC pulses. Pump and probe/reference beams are crossed in a chamber filled with N_2 , O_2 , or Ar. The spectral phase and amplitude of the probe is measured and used to find the time-domain phase shift induced by the pump pulse.

The crossing angle is small enough to consider all pulses as collinear in the analysis. The reference pulse precedes the pump, which is temporally overlapped by the probe, which is encoded with the pump-induced time-varying nonlinear phase shift. The focal plane of the reference/probe is imaged onto the entrance slit of an imaging spectrometer, inside of which the reference and probe pulses interfere in the spectral domain. Two-dimensional spectral interferograms (1D space and wavelength) are recorded by a CCD camera at the spectrometer's imaging plane. The 2° angular separation between the pump and reference/probe ensures that the pump is stopped at a beam dump before the entrance slit. Fourier analysis of the spectral interferogram, using the measured spectral phase of the probe [23, 24], enables extraction of the time- and 1D space-resolved phase shift $\Delta\varphi(x, t)$ induced by the pump pulse with the time resolution limited to <5 fs by the SC bandwidth. Here, x is a transverse coordinate in the pump focal plane.

The reference/probe polarization is oriented either parallel or perpendicular to the pump polarization by a half waveplate before the xenon SC cell. A Glan-Taylor polarizer ($10^5:1$ extinction ratio) is placed in the reference/probe path to further refine the linear polarization. Pump-probe walk-off is minimal in these experiments: for the probe central wavelength $\lambda_p = 600$ nm and pump wavelength range $\lambda_e = 400\text{--}2400$ nm, the walkoff for our pump-probe interaction length of ~ 2 mm is < 0.5 fs, well below the time scale of the most rapid index transients in the experiment, which are of order the pulse width of 40 fs (at $\lambda_e = 800$ nm).

In N_2 and O_2 , the nonlinear response is dominated by the near-instantaneous electronic (Kerr) and the delayed rotational responses [24]. If $\Delta\varphi_{\parallel}(x, t) = \Delta\varphi_{elec}(x, t) + \Delta\varphi_{rot}(x, t)$ is the SSSI-extracted phase shift for the parallel polarized probe, then nonlinear susceptibility tensor symmetry [25] implies that $\Delta\varphi_{\perp}(x, t) = \frac{1}{3}\Delta\varphi_{elec}(x, t) - \frac{1}{2}\Delta\varphi_{rot}(x, t)$ for the perpendicular polarized probe. These equations then yield

$$\begin{aligned}\Delta\varphi_{elec}(x, t) &= 3(\Delta\varphi_{\parallel}(x, t) + 2\Delta\varphi_{\perp}(x, t)) / 5 \\ \Delta\varphi_{rot}(x, t) &= 2(\Delta\varphi_{\parallel}(x, t) - 3\Delta\varphi_{\perp}(x, t)) / 5\end{aligned}\quad (1)$$

for the separate electronic and rotational nonlinear responses.

Figures 2(a) and 2(b) show $\Delta\varphi_{\parallel}(x, t)$ and $\Delta\varphi_{\perp}(x, t)$ phase shift measurements in nitrogen at $\lambda_e = 1250$ nm pump wavelength. Central lineouts $\Delta\varphi_{\parallel}(0, t)$ and $\Delta\varphi_{\perp}(0, t)$ are shown in (c), along with the electronic and

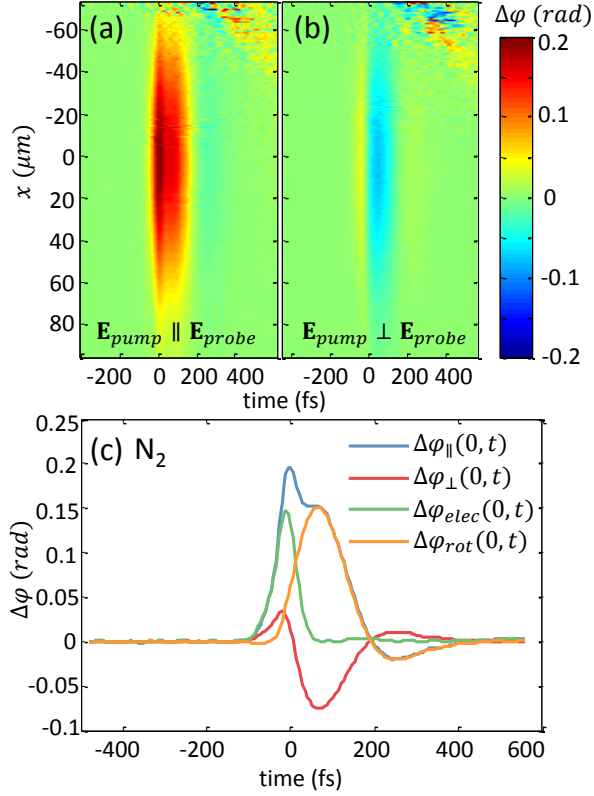


Fig. 2. Experimental results in N_2 at $\lambda_e = 1250$ nm central pump wavelength. (a) Nonlinear phase shift $\Delta\varphi_{||}(x,t)$ of the probe for $\mathbf{E}_{pr} \parallel \mathbf{E}_{pump}$ and (b) nonlinear phase shift $\Delta\varphi_{\perp}(x,t)$ of the probe for $\mathbf{E}_{pr} \perp \mathbf{E}_{pump}$ (c) Temporal lineouts $\Delta\varphi_{||}(0,t)$ and $\Delta\varphi_{\perp}(0,t)$ and their decomposition into electronic and rotational responses, as described in the text.

Rotational responses $\Delta\varphi_{elec}(0,t)$ and $\Delta\varphi_{rot}(0,t)$ extracted using Eq. (1). Figure 3 shows the same plot for argon, which lacks a rotational response, verifying that $\Delta\varphi_{elec,||}(0,t) = 3\Delta\varphi_{elec,\perp}(0,t)$ in accord with the symmetry of an instantaneous isotropic nonlinearity. This result verifies the sensitive ability of our technique to separate the electronic and rotational responses in molecular gases.

Our prior absolute determination of the Kerr and rotational nonlinearities at $\lambda = 800$ nm used auxiliary interferometric measurements of the optical thickness of our thin gas target and measurements of the pump intensity profile [19]. Here, we use an alternative method, employed in other recent pump-probe nonlinearity measurements [26, 27], in which we reference all of our nonlinear phase shift measurements to the rotational responses in nitrogen and oxygen without explicit need for either gas density or pump intensity profiles. We use the fact that, to second order in the pump field, the response, as measured by the nonlinear index shift experienced by the probe, is the sum of the electronic and rotational responses [19],

$$\Delta n_p(x,t) = 2n_2 I(x,t) + \int_{-\infty}^t R(t-t') I(x,t') dt' \quad (2)$$

where I is the pump intensity, n_2 is the electronic Kerr coefficient, which depends on the probe and pump wavelengths λ_p and λ_e , and R is the impulse response function for quantized rotations of a rigid rotor. The terms in Eq. (2) are related to our measured phase shifts by

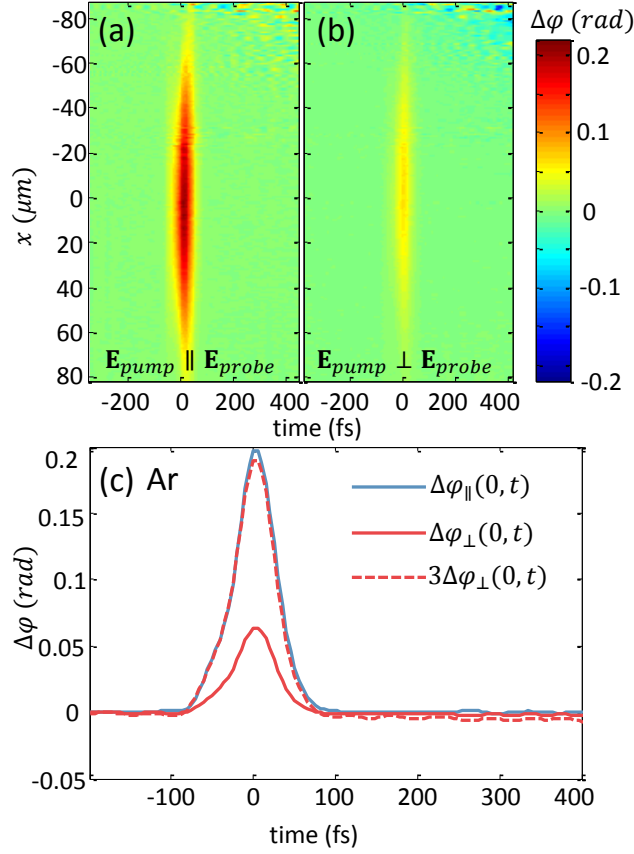


Fig. 3. Experimental results in Ar at 1250 nm pump central wavelength: (a) $\Delta\varphi_{||}(x, t)$ and (b) $\Delta\varphi_{\perp}(x, t)$. (c) Temporal lineouts of the parallel and perpendicular polarized phase shift and the perpendicular phase shift scaled by a factor of 3.

$$\begin{aligned}
\Delta\varphi_{elec}(x, t) &= 2n_2 I_0 f(x, t) k_p L \\
\Delta\varphi_{rot}(x, t) &= \frac{2\pi N k_p L}{n_0} \Delta\alpha(\lambda_p) \langle \cos^2 \theta \rangle_t - \frac{1}{3} \\
&= \frac{2\pi N k_p L}{n_0} \Delta\alpha(\lambda_p) \frac{\Delta\alpha(\lambda_e) I_0}{ch} \int_{-\infty}^t g(t-t') f(x, t') dt'
\end{aligned}$$

(3)

where I_0 is the pump peak intensity and $f(x, t)$ is its normalized spatiotemporal profile, k_p is the probe wavenumber, $L \sim 2$ mm ($<$ pump confocal parameter of ~ 5 cm) is the pump-probe interaction length, N is the molecule number density, n_0 is the background gas refractive index, $\Delta\alpha(\lambda_e)$ ($\Delta\alpha(\lambda_p)$) is the polarizability anisotropy at the pump (probe) wavelength, $\langle \cos^2 \theta \rangle_t - \frac{1}{3}$ is the ensemble-averaged transient alignment induced by the pump pulse [24], and the rescaled impulse response function is [24]

$$g(t) = \frac{-16\pi}{15} \sum_j \frac{j(j-1)}{2j-1} (\rho_j^{(0)} - \rho_{j-2}^{(0)}) \sin \omega_{j, j-2} t \quad (4)$$

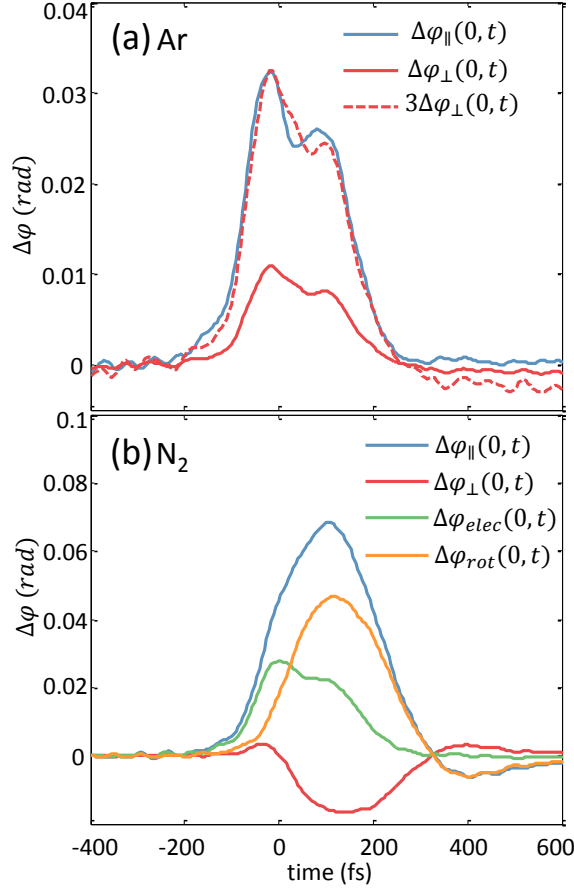


Fig. 4. Experimental results in (a) Ar and (b) N₂ at 2200 nm, a wavelength where the pump pulse shape is longer and more complex than at shorter wavelengths.

where $\rho_j^{(0)}$ is the thermal population of state j , $\omega_{j,j-2} = 4\pi B(2j-1)$, and B is the rotational constant.

Essential to our method for absolute measurements is accurate recovery of the pump pulse envelope. Figures 4(a) and (b) show the nonlinear phase shift at $\lambda_e = 2200$ nm for argon and nitrogen. The somewhat complex pulse pump envelope $f(x,t)$ measured in (a) results from the propagation of the OPA idler through a dichroic mirror. Figure 4(b) shows that such accurate recovery of the intensity envelope enables a clean separation of the electronic and rotational responses, even when the envelope is complex. Examination of Eq. (3) now shows that measurement of $\Delta\phi_{rot}$ and computation of the convolution integral $\int_{-\infty}^t g(t-t')f(x,t')dt'$ from the known and measured functions g and f gives $\mu_1 = \Delta\alpha(\lambda_p)\Delta\alpha(\lambda_e)NLI_0$. This then allows determination of $\mu_2 \equiv n_2(\Delta\alpha(\lambda_p)\Delta\alpha(\lambda_e))^{-1}$ through the equation for $\Delta\phi_{elec}(x,t)$. It is important to note that there is a large two-dimensional sample size of μ_2 measurements in each SSSI shot, since the phase shift measurement is both time and 1D-space resolved. In the extracted phases shown here (for example, Fig. 2) there are ~ 100 points in x and ~ 50 -100 points in t , so in principle each shot embodies a maximum ~ 5000 measurements of μ_2 .

Our results are summarized in Table 1. The uncertainties quoted in the table originate from three sources. First is the residual square error in μ_1 from least squares fits of $\Delta\phi_{rot}(x,t)$ (Eq. (3)) to the data points spanning t for fixed x . The x -average of these results gives the tabulated n_2 values, and the standard deviation is one source of uncertainty. Another source of uncertainty is slight laser average power drift over the course of a run, and we include its estimated effect in the displayed error. Finally, we include the propagated uncertainty

in the value of $\Delta\alpha$, as given in [19]. The noticeably higher error for the $\lambda_e=2400$ nm measurements originates from the very small nonlinear phase shifts (maximum of ~ 30 mrad) measured for that low peak pump intensity.

From the expression above for μ_2 it is clear that determination of n_2 requires assessment of dispersion in $\Delta\alpha$. Such dispersion has been calculated to have the approximate frequency dependence $\Delta\alpha(\omega) \approx \Delta\alpha(0) + C\omega^2$ [28]. Light scattering measurements for N_2 [29] are well fit by $\Delta\alpha(0) = 6.6 \times 10^{-25} \text{ cm}^3$ and $C = 3.8 \times 10^{-57} \text{ cm}^3\text{s}^2$. This relation, with $\Delta\alpha(0)$ scaled so that $\Delta\alpha(\omega)$ matches our measured value of $\Delta\alpha$ at $\lambda_e=800$ nm [19], was used to account for the dispersion of $\Delta\alpha$ in the analysis. The dispersion is quite weak: $\Delta\alpha(\omega_{800\text{nm}})/\Delta\alpha(0) \sim 1.03$ and $\Delta\alpha(\omega_{400\text{nm}})/\Delta\alpha(0) \sim 1.13$.

It is evident from Table 1, that neglecting $\Delta\alpha$ dispersion affects the results by at most $\sim 10\%$ near $\lambda=400$ nm and $<2\%$ at longer wavelengths (compare columns (a) and (b)). Next, we see that results for n_2 are dispersionless within the precision of our measurements, except near $\lambda_e=400$ nm (except for O_2). This is in accord with calculations of the third order hyperpolarizability at optical frequencies below electronic resonances [21, 30]. It is important to be clear that while the Kerr coefficient we actually desire is $n_2(\omega_e) = (12\pi^2 / n_0^2 c) N \gamma^{(3)}(\omega_e; \omega_e, -\omega_e, \omega_e)$, where $\gamma^{(3)}$ is the third order hyperpolarizability, our pump-probe experiment actually measures $n_2(\omega_e, \omega_p) \propto \gamma^{(3)}(\omega_p; \omega_e, -\omega_e, \omega_p)$. However, the $\gamma^{(3)}$ dispersion formula of [21] and its parametrization by Shelton and Rice [30] give

$$\gamma^{(3)}(\omega_s; \omega_1, \omega_2, \omega_3) = \gamma_0 (1 + a\omega_L^2 + b\omega_L^4 + \dots), \quad (5)$$

where $\omega_s = \omega_1 + \omega_2 + \omega_3$, γ_0 is the static hyperpolarizability, $\omega_L^2 = \omega_s^2 + \omega_1^2 + \omega_2^2 + \omega_3^2$, and $a=1.8 \times 10^{-33}$, $3 \times 10^{-33} \text{ s}^2$, $b=1.5 \times 10^{-65}$, $1.6 \times 10^{-65} \text{ s}^4$ and $\gamma_0 = 7.7 \times 10^{-30}$, $9.8 \times 10^{-30} \text{ cm}^6\text{W}^{-1}\text{s}^{-1}$ for N_2 and Ar respectively. For our pump-probe case, $\omega_L^2 = 2\omega_e^2 + 2\omega_p^2$ and Eq. (5) gives, at worst (shortest λ_p and longest λ_e), $\delta = |(n_2(\omega_e, \omega_p) - n_2(\omega_e)) / n_2(\omega_e)| < \sim 0.06$ for pump and probe wavelengths longer than ~ 500 nm, which applies to most of Table I and is within our measurement error. For $\lambda_e=400$ nm and $\lambda_p=600$ nm (peak of SC), $\delta < \sim 0.06$, also within our measurement error, confirming the dispersion of n_2 in N_2 and Ar near 400 nm.

In Table 1, we compare our results in Ar, N_2 , and O_2 with the values of n_2 calculated with Eq. (5) using values of γ_0 , a , and b (shown above for N_2 and Ar) found using the electric field induced second harmonic generation (ESHG) technique [31], in which $\omega_1 = \omega_2 = \omega$ and $\omega_3 = 0$. The agreement is very good. The ESHG results in argon and nitrogen [31] have been shown to agree with theoretical calculations [32,33] to within $\sim 10\%$. Both theory and ESHG experiments agree with our finding that the nonlinear refractive index is quite dispersionless in the infrared. For application of these results to propagation simulations, both the electronic and rotational contributions must be considered as shown in Eq. (2). For short pump pulses in N_2 and O_2 ($< \sim 50$ fs), the electronic response dominates and for longer pulses ($> \sim 150$ fs), the rotational response dominates, as inferred directly from Figs. 2 and 4. In the limit of a very long pulse, the molecular response is adiabatic, and the effective nonlinearity coefficient can be written as $n_{2,\text{eff}} = n_2 + n_{2,\text{rot}}$, where calculated values of $n_{2,\text{rot}}$ (using our measured values of $\Delta\alpha$ [19]) are shown in Table 1.

In conclusion, we have used single shot supercontinuum spectral interferometry to measure the electronic Kerr coefficients for the major atmospheric constituents, N_2 , O_2 and Ar, at wavelengths ranging from 400 nm to 2400 nm. Our measurements are referenced to the polarizability anisotropy of the molecular gases, which enables extraction of absolute nonlinearities without the need for separate measurements of the gas density or pump intensity profiles. Except for the nitrogen and argon measurements at pump wavelength near 400 nm, the Kerr coefficients are measured to be dispersionless within the precision of our apparatus and consistent with the theoretical predictions.

Pump wavelength λ_e (nm)	(a) N ₂			(b) N ₂			(c) O ₂			(d) Ar	
	n_2 ($10^{-20} \text{ cm}^2/\text{W}$)			n_2 ($10^{-20} \text{ cm}^2/\text{W}$)			n_2 ($10^{-20} \text{ cm}^2/\text{W}$)			n_2 ($10^{-20} \text{ cm}^2/\text{W}$)	
	This work	[28]	$n_{2,rot}$	This work	[28]	$n_{2,rot}$	This work	[28]	$n_{2,rot}$	This work	[28]
400 nm	10.1±1.2	9.4	29	9.3±1.1		24	8.5±0.8	10.8	54	10.9±1.3	12.2
800 nm	7.9±0.8	8.4	24	7.9±0.8		24	8.1±0.7	9.0	54	10.1±1.0	10.7
1250 nm	7.7±0.7	8.2	23	7.9±0.8		24	8.9±0.7	8.8	54	10.5±1.4	10.5
1650 nm	8.0±0.8	8.1	23	8.1±0.8		24	7.9±0.6	8.7	54	10.9±1.0	10.4
2200 nm	7.2±0.8	8.1	23	7.4±0.8		24	8.2±0.8	8.6	54	9.3±1.0	10.4
2400 nm	7.6±1.3	8.1	23	7.8±1.3		24	10.0±1.2	8.6	54	9.9±1.7	10.3

(a) n_2 measurements are adjusted for $\Delta\alpha$ dispersion using coefficients found in [29]

(b) n_2 measurements are not adjusted for $\Delta\alpha$ dispersion. We used $\Delta\alpha(\omega_{800nm})$, measured in [19], for all wavelengths.

(c) n_2 measurements are not adjusted for $\Delta\alpha$ dispersion.. We used $\Delta\alpha(\omega_{800nm})$, measured in [19], for all wavelengths.

(d) Referenced to N₂ measurements.

Table 1. Measured values of n_2 (“This work”) of major air constituents, scaled to atmospheric pressure. Comparison is shown to values of n_2 calculated for our wavelengths using Eq. (5), where the coefficients a , b , and γ_0 were measured using the ESHG technique [28]. For long pulses, the effective nonlinearity coefficient can be written as $n_{2,eff} = n_2 + n_{2,rot}$.

The authors thank Eric Rosenthal, Nihal Jhaji, and Ilia Larkin for useful discussions and technical assistance. The authors also thank M. Kolesik for theoretical discussions. This work was supported by the Air Force Office of Scientific Research (AFOSR), the Army Research Office (ARO), and the National Science Foundation (NSF).

REFERENCES

1. A. Couairon and A. Mysyrowicz, "Femtosecond filamentation in transparent media," Phys. Rep. **441**, 47, pp. 47-189 (2007).
2. L. Berge, S. Skupin, R. Nuter, J. Kasparian, and J.-P. Wolf, "Ultrashort filaments of light in weakly ionized, optically transparent media," Rep. Prog. Phys. **70**, pp. 1633-1713 (2007).
3. K. Y. Kim, A. J. Taylor, J. H. Glowina and G. Rodriguez, "Coherent control of terahertz supercontinuum generation in ultrafast laser-gas interactions," Nature Photon. **2**, pp. 605-609 (2008)
4. T. Vockerodt, D. S. Steingrube, E. Schulz, M. Kretschmar, U. Morgner and M. Kovačev, "Low- and high-order harmonic generation inside an air filament," Appl. Phys. B **106**, 3, pp. 529-532 (2012)
5. Y. Liu, Y. Brelet, G. Point, A. Houard, and A. Mysyrowicz, "Self-seeded lasing in ionized air pumped by 800 nm femtosecond laser pulses," Opt. Express **21**, 19, pp. 22791-22798 (2013).
6. D. Kartashov, S. Ališauskas, A. Baltuška, A. Schmitt-Sody, W. Roach, and P. Polynkin, "Remotely pumped stimulated emission at 337 nm in atmospheric nitrogen," Phys. Rev. A **88**, 041805 (2013)
7. A. Dogariu, J. B. Michael, M. O. Scully, R. B. Miles, "High-Gain Backward Lasing in Air," Science **331**, 6016 pp. 442-444 (2011)
8. Y.-H. Cheng, J. K. Wahlstrand, N. Jhaji, and H. M. Milchberg, "The effect of long timescale gas dynamics on femtosecond filamentation," Opt. Express **21**, pp. 4740-4751 (2013); N. Jhaji, Y.-H. Cheng, J. K. Wahlstrand, and H. M. Milchberg, "Optical beam dynamics in a gas repetitively heated by femtosecond filaments," Opt. Express **21**, pp. 28980-28986 (2013).

9. N. Jhajj, E. W. Rosenthal, R. Birnbaum, J. K. Wahlstrand, and H. M. Milchberg, "Demonstration of Long-Lived High-Power Optical Waveguides in Air," *Phys. Rev. X* **4**, 011027 (2014).
10. E. W. Rosenthal, N. Jhajj, J. K. Wahlstrand, and H. M. Milchberg, "Collection of remote optical signals by air waveguides," *Optica* **1**, 1, pp. 5-9 (2014).
11. J. K. Wahlstrand, N. Jhajj, E. W. Rosenthal, S. Zahedpour, and H. M. Milchberg, "Direct imaging of the acoustic waves generated by femtosecond filaments in air," *Opt. Lett.* **39**, pp. 1290-1293 (2014).
12. N. Jhajj, J. K. Wahlstrand, and H. M. Milchberg, "Optical mode structure of the air waveguide," *Opt. Lett.* **39**, pp. 6312-6315 (2014).
13. O. Lahav, L. Levi, I. Orr, R. A. Nemirovsky, J. Nemirovsky, I. Kaminer, M. Segev, and O. Cohen, "Long-lived waveguides and sound-wave generation by laser filamentation," *Phys. Rev. A* **90**, 021801 (2014).
14. P. Panagiotopoulos, P. Whalen, M. Kolesik, and J. V. Moloney, "Super high power mid-infrared femtosecond light bullet," *Nature Photon.* **9**, pp. 543-548 (2015).
15. T. Popmintchev, M.-C. Chen, D. Popmintchev, P. Arpin, S. Brown, S. Ališauskas, G. Andriukaitis, T. Balčiūnas, O. D. Mücke, A. Pugžlys, A. Baltuška, B. Shim, S. E. Schrauth, A. Gaeta, C. Hernández-García, L. Plaja, A. Becker, A. Jaron-Becker, M. M. Murnane, H. C. Kapteyn, "Bright coherent high harmonics in the keV X-ray regime from mid-infrared femtosecond lasers," *Science* **336**, pp. 1287-1291 (2012).
16. D. Kartashov, S. Ališauskas, A. Pugžlys, A. Voronin, A. Zheltikov, M. Petrarca, P. Béjot, J. Kasparian, J. P. Wolf, and A. Baltuška, "Mid-infrared laser filamentation in molecular gases," *Opt. Lett.* **38**, 16 pp. 3194-3197 (2013).
17. A. Couairon and L. Berge, *Phys. Plasmas* **7**, 193 (2000); M. Kolesik and J. V. Moloney, "Modeling and simulation techniques in extreme nonlinear optics of gaseous and condensed media," *Rep. Prog. Phys.* **77**, 016401 (2014); J.P. Palastro, T. M. Antonsen, S. Varma, Y.-H. Chen, and H. M. Milchberg, "Simulations of femtosecond atmospheric filaments enhanced by dual pulse molecular alignment," *Phys. Rev. A* **85**, 043843 (2012).
18. E. W. Rosenthal, J. P. Palastro, N. Jhajj, S. Zahedpour, J. K. Wahlstrand, and H. M. Milchberg, "Sensitivity of propagation and energy deposition in femtosecond filamentation to the nonlinear refractive index," *J. Phys. B* **48**, 094011 (2015).
19. J. K. Wahlstrand, Y. H. Cheng, H. M. Milchberg, "Absolute measurement of the transient optical nonlinearity in N_2 , O_2 , N_2O , and Ar" *Phys. Rev. A* **85**, 043820 (2012).
20. D. A. Simons and A. Tokunaga, "The Mauna Kea Observatories Near-Infrared Filter Set. I: Defining Optimal 1-5 μm Bandpasses" *Publ. Astron. Soc. Pac.* **114**, (2002).
21. D. M. Bishop, "General dispersion formulas for molecular third-order nonlinear optical properties," *J. Chem. Phys.* **90**, pp. 3192-3195 (1989).
22. HE-TOPAS, Light Conversion
23. K. Y. Kim, I. Alexeev, and H. M. Milchberg, "Single-shot supercontinuum spectral interferometry," *Appl. Phys. Lett.* **81**, pp. 4124-4126 (2002)
24. Y.-H. Chen, S. Varma, A. York, and H. M. Milchberg, "Single-shot, space- and time-resolved measurement of rotational wavepacket revivals in H_2 , D_2 , N_2 , O_2 , and N_2O ," *Opt. Express* **15**, pp. 11341-11357 (2007).
25. R. L. Sutherland, *Handbook of Nonlinear Optics* (Marcel Dekker, New York, 1996).
26. V. Loriot, E. Hertz, O. Faucher, and B. Lavorel, "Measurement of high order Kerr refractive index of major air components," *Opt. Express* **17**, 13429-13434 (2009).
27. M. Reichert, P. Zhao, J. M. Reed, T. R. Ensley, D. J. Hagan, and E. W. van Stryland, "Beam deflection measurement of bound-electronic and rotational nonlinear refraction in molecular gases," *Opt. Express* **23**, 22224-22237 (2015).

28. M. A. Spackman, "Time-dependent Hartree–Fock second-order molecular properties with a moderately sized basis set. I. The frequency dependence of the dipole polarizability," *J. Chem. Phys.* **94**, pp. 1288-1294 (1991).
29. G. R. Alms, A. K. Burnham, and W. H. Flygare, "Measurement of the dispersion in polarizability anisotropies," *J. Chem. Phys.* **63**, pp. 3321-3326 (1975).
30. D. P. Shelton and J. E. Rice, "Measurements and calculations of the hyperpolarizabilities of atoms and small molecules in the gas phase," *Chem. Rev.* **94**, pp. 3–29 (1994).
31. D. P. Shelton, "Nonlinear-optical susceptibilities of gases measured at 1064 and 1319 nm," *Phys. Rev. A* **42**, pp. 2578-2592 (1990).
32. J. E. Rice, "Frequency-dependent hyperpolarizabilities for argon, krypton, and neon: Comparison with experiment," *J. Chem. Phys.* **96**, pp. 7580-7586 (1992).
33. H. Sekino and R. J. Bartlett, "Hyperpolarizabilities of molecules with frequency dependence and electron correlation," *J. Chem. Phys.* **94**, 3665-3669 (1991); H. Sekino and R. J. Bartlett, "Molecular hyperpolarizabilities," *J. Chem. Phys.* **98**, pp. 3022-3077 (1993).